RESEARCH ARTICLE

Correlations between slow pyrolysis characteristics and organic carbon structure of aquatic plant biomass

Lei Xu [1,2,3] · Fei Guo [1,2,3] · Guojing Wang [1] · John P. Giesy [1,4] · Yingchen Bai [1] · Xianglian Wang [2,3] · Fanhao Song [1]

Abstract

Thermal analysis techniques have been widely used to characterize natural organic matter; in particular, thermal oxidation has been used to examine soil and sediment organic matter. However, few studies have characterized natural organic matter (NOM) by using slow thermal degradation under a N_2 atmosphere. ^{13}C nuclear magnetic resonance (NMR) spectroscopy, UV-Vis spectroscopy, and three-dimensional excitation and emission matrix (EEM) fluorescence spectroscopy were used to characterize aquatic plant biomass for the detailed interpretation of the structures of organic carbon during slow pyrolysis. There was a significant linear correlation between the absorption of heat (99–110 °C) and the loss of mass (110–160 °C) ($r^2 = 0.507$, $p = 0.01$), which indicates that the initial slight loss in mass of the plant materials was due to the loss of less thermally stable components. The release of heat (277–311 °C) and the ratio of the specific absorbances at 253 and 203 nm ($A_{253/203}$) were also correlated ($r^2 = 0.388$, $p = 0.008$), which suggests that the release of plant biomass upon heating was associated with the proportion of substituent groups on aromatic rings and that the release of heat increased with the amount of substitution. The coefficient of determination (r^2) between fulvic acid-like fluorescence peaks and the loss of mass (230–340 °C) was 0.236 ($p = 0.048$). This result indicates that the loss of mass in the plant material samples was related to fulvic acid-like substances. More specifically, the reason for this result was the splitting of some aromatic functional groups, such as ether bonds, carbonyl groups, and oxygen heterocycles. In conclusion, these results suggest that the developed correlations between slow pyrolysis characteristics and organic carbon structures contribute to the investigation of the inner chemical structures of natural organic matter.

Keywords Lake aquatic macrophytes · Tai Lake · ^{13}C NMR spectroscopy · UV-vis spectroscopy · EEM fluorescence spectroscopy · Asia

Introduction

Natural organic matter (NOM) is an important component of various environmental media as well as a significant part of the global carbon cycle. NOM is a constituent of important segments of ecological systems and plays a significant role in the transformation of energy and material cycles in ecosystems (Jansson 1998). Therefore, it is necessary to characterize the forms and environmental behaviors of NOM. In recent years, researchers have used thermal techniques, including differential thermal analysis (DTG) and differential scanning calorimetry (DSC), to characterize the oxidation of organic matter. Compared to conventional methods, thermal analyses have advantages, including rapidity, little required pretreatment of samples, and the ability to obtain reliable results (Aiken and Hsu 2011).

Most studies have focused on the thermal stability of soil organic matter and plant biomass under aerobic conditions or

have determined the mechanisms and products of thermal degradation of biomass at a fixed temperature under an anaerobic atmosphere. There have been qualitative descriptions of the behaviors of soil and sediment organic matter during slow thermal oxidation, and some investigators have reported that decomposition of soil organic carbon can be divided into three stages: first, the decomposition of labile organic matter, followed by the degradation of more recalcitrant organic matter, and finally, the decomposition of the most refractory organic matter (Dell'Abate et al. 2015; Lopez-Capel et al. 2006). To investigate differences in thermal stability and composition at different temperatures, soil humic substances have been characterized by TGA and DSC. These studies confirmed that thermal analysis can be used to distinguish among forms of vegetation (Antisari et al. 2010). Organic matter in the litter layer of forests after shrub fires has been successfully characterized by using DSC (Alexis et al. 2010). When compost from vegetable waste during several seasons was characterized under aerobic conditions, two exothermic phases were observed. One was the evaporation of aliphatic compounds and carbohydrates, while the other was the oxidation of components of greater molecular mass (Ali et al. 2012).

NOM research using thermal degradation in an anaerobic (N_2) atmosphere is limited. Some studies have qualitatively explored the characteristics of slow pyrolysis, while others have used thermal oxidation. Thermal techniques (DTG and TGA) have been applied to study the biodegradation of tannery wastes in an N_2 atmosphere. In that study, there were two main endothermic peaks: one was observed between 300 and 380 °C, while the other was observed in the range of 450–550 °C (Ravindran et al. 2013). Thermal and spectral techniques have been used to characterize the thermal behavior, under an anaerobic atmosphere, of sediment collected in cores and there were two main thermal degradation processes that could be observed in thermograms. These were interpreted to represent labile organic carbon and more recalcitrant organic carbon. The thermal stability of labile and recalcitrant organic carbon increased gradually with age (Guo et al. 2016a). Most previous analyses have been based on the interpretation of slow pyrolysis curves. During slow pyrolysis, it is also possible to obtain quantitative parameters, such as heat absorption, release of heat, and rate of loss of mass.

Other advanced techniques have also been used to characterize the chemical compositions and structural characteristics of natural organic matter, including ^{13}C NMR spectroscopy, UV-Vis spectroscopy, and EEM fluorescence spectroscopy. Dissolved organic matter (DOM) derived from 13 plant biomass and animal manure sources was characterized using EEM fluorescence spectroscopy. The results showed that there were seven fluorescence components (tryptophan-like, tyrosine-like, and five humic substance-like components) in DOM derived from plants and manure, and decomposition significantly affected the concentration of three humic substance-like-associated components for most of the plant-derived DOM solutions (And and Ohno 2007). The characteristics of the absorbance spectra of chromophoric dissolved organic matter (CDOM) from cave and spring waters were investigated by using UV-Vis and EEM spectroscopy. The results showed that the origin of cave and spring CDOM appeared to be from microbially derived materials, and the degree of OM humification was low, based on fluorescence-derived indices and absorbance spectral characteristics (Birdwell and Engel 2010). The structures of humic substances in fresh waters were characterized using ^{13}C NMR spectroscopy; the results showed that the carboxyl and aromatic carbon contents of Lake Celyn humic acid were 24% and 40%, respectively, and the humic acid was largely formed from terrestrial humic substances (Wilson et al. 1981).

Slow pyrolysis has the advantages of being rapid, convenient, and quantitative, but due to the complexities of NOM, theories and interpretations of the results of slow pyrolysis to characterize NOM are limited. Hence, it has not been easy to interpret thermal degradation curves and determine corresponding component features. However, spectroscopy can be used to qualitatively characterize the chemical composition and structural characteristics of NOM. To more completely characterize NOM, thermal and spectroscopic techniques have therefore been combined, and we noticed that the relationship between the characteristics of slow pyrolysis and the spectra of biomass has not been emphasized owing to the limited number of plants. In this paper, ^{13}C NMR, UV-Vis, and EEM fluorescence spectroscopy were combined with thermal techniques to characterize 17 plant samples into four categories. We have carefully studied the relationship between the spectroscopic characteristics and slow pyrolysis characteristics of plant biomass. The objective of this study was to investigate the mechanism of the slow pyrolysis of biomass from aquatic macrophytes through an analysis of the relationships between plant biomass structures containing organic carbon and the characteristics of slow pyrolysis; the results contribute to further understanding of the stability of organic carbon and the intrinsic structure of NOM.

Materials and methods

Sample collection and pretreatment

Seventeen samples of various lacustrine plants were obtained from Tai Lake (Taihu in Chinese) east of Jiangsu Province, China. We collected mature plants and leaves, stems, and roots of plants at the same time to avoid negative influence from different growth stages and organs. The plants were classified as emergent, submerged, floating, or terrestrial. Whole-plant samples were well mixed and killed at 90 °C for 1–2 h, then thoroughly dried at 60 °C for 12 h, and then sieved to 1 mm.

Elemental analysis

For measurement of the total contents of carbon (C), hydrogen (H), oxygen (O), nitrogen (N), and sulfur (S), 10 g of freeze-dried plant samples was detected with an Elementar vario macro EL. The atmosphere was 0.2 MPa He and 0.25 MPa O_2 for all elements; other operating parameters of elemental analysis were applied according to a previous study (Lin et al. 2011).

^{13}C nuclear magnetic resonance

^{13}C NMR spectra were collected by placing approximately 100 mg of sample into a Bruker DRX 400 NMR spectrometer (Germany) in which the spinning rate was 106 MHz and the acquisition parameters included a pulse delay time of 5 s and a pulse width of 4.5 ms (Lin et al. 2011).

UV-Vis spectroscopy

Aliquots of 1 mg of plant materials were dissolved in 40 ml of 0.05 M $NaHCO_3$, and the pH was adjusted to 8.0. UV-Vis absorption spectra were collected by using an Agilent 8453 UV-Vis spectrophotometer (Prado et al. 2011) in a wavelength range from 200 to 800 nm. Absorbance values at 203, 254, 280, 365, 465, and 665 nm were recorded to evaluate the UV-Vis parameters A_{253}/A_{203}, A_{250}/A_{365}, and A_{465}/A_{665} (Lin et al. 2011).

EEM fluorescence spectroscopy

Aliquots of 1 mg of plant materials were dissolved in 40 ml of 0.05 M $NaHCO_3$, and the pH was adjusted to 8.0. All EEM spectra were measured by using luminescence spectrometry (F-7000, Hitachi Ltd., Japan). EEM spectra are a series of emission spectra over a range of excitation wavelengths, which can be used to identify fluorescent compounds present in complex mixtures (Sheng and Yu 2006). In this experiment, EEM spectra were collected by subsequent scanning of emission spectra from 200 to 600 nm at increments of 0.5 nm by varying the excitation wavelength from 200 to 400 nm at increments of 10 nm. Slit widths were maintained at 10 nm for both excitation and emission, and the scanning speed was 1200 nm min^{-1} for all measurements (Lin et al. 2011).

Thermal gravimetric analysis

Thermal gravimetric analyses were performed by using a TGA Q50 thermogravimetric analyzer (TA Instruments, USA) to record the thermal stability of plant samples. The maximum experimental temperature was 1000 °C. More experimental parameters were provided elsewhere (Guo et al. 2016b).

Differential scanning calorimetry

Differential scanning calorimetry was performed by using a DSC Q20 differential scanning calorimeter (TA Instruments). The maximum experimental temperature was 600 °C. More detailed experimental parameters are given elsewhere (Guo et al. 2016b).

Results

^{13}C NMR spectral characteristics

While there were some similarities, the NMR spectra varied among the plant materials (Fig. 1 and Table 1). The spectra all exhibited a large peak in the range of 70 to 100 ppm, which indicated acetal carbon atoms in carbohydrates. The following chemical shifts in the ^{13}C NMR spectra were identified and integrated: aliphatic carbons in the region of 0–110 ppm (more specifically, 0–45 ppm, paraffinic carbons; 45–65 ppm, methoxy groups; and 65–110 ppm, alcohol and acetal groups), aromatic carbons in the region of 110–160 ppm (more specifically, 110–145 ppm, aromatic groups; and 145–160 ppm, phenolic groups), carboxyl groups in the region of 160–190 ppm, and carbonyl groups in the region of 190–230 ppm (And and Xing 2008).

In the region of aliphatic carbons (0–110 ppm), the mean content of aliphatic carbons of terrestrial plants was 83.32%, which was greater than that of emergent plants, submerged plants, and floating plants (81.17%, 81.52%, and 79.44% by mass, respectively). The four types of plants contained a predominance of aliphatic carbon groups with oxygen (40–110 ppm), accounting for 53.69%, 54.18%, 49.53%, and 47.09% by mass, respectively. In the region of the spectra representing aromatic carbons (110–160 ppm), the mean content of aromatic carbons in emergent plants was 11.40%, which was greater than that in terrestrial plants, floating plants, and submerged plants, which had contents of 7.85%, 10.47%, and 9.03%, respectively. In all types of plants studied, the contents of aromatic-group carbons were higher than those of phenolic-group carbons. In the regions of the spectra that represent carboxyl carbons (160–190 ppm) and carbonyl carbons (190–230 ppm), the mean contents of carboxyl carbons and carbonyl carbons were the greatest in floating plants, whereas those in emergent plants were the least. The contents in these two types of plants were 10.25% and 7.51%, respectively. Among all plants studied, the content of carboxyl carbons was greater than that of carbonyl carbons. This quantitative information about the organic carbon structure distribution could provide a reference for the interpretation of pyrolysis and a better understanding of the composition of biomass.
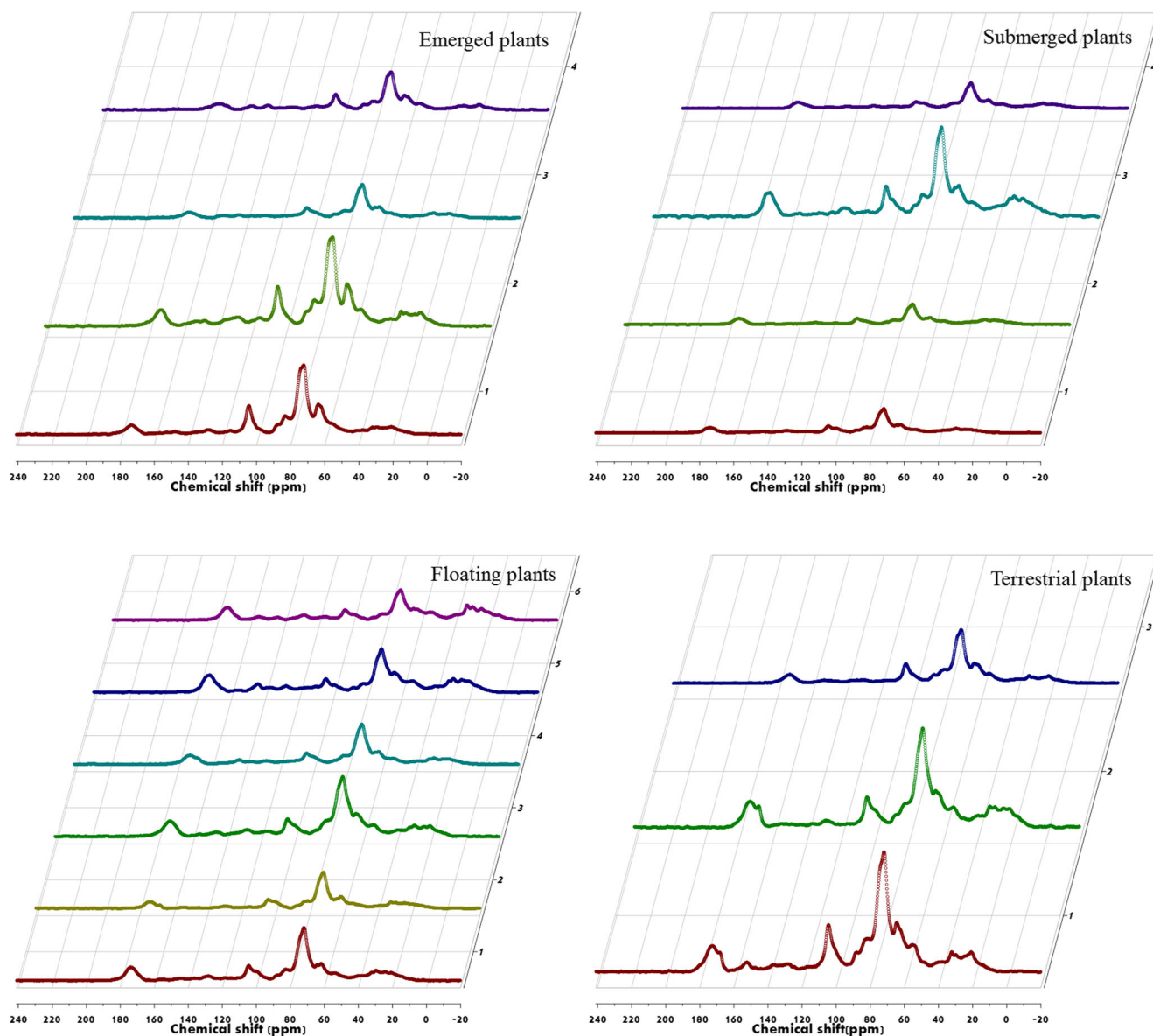
Fig. 1 ^{13}C NMR spectra of lacustrine plants

UV-Vis spectral characteristics

UV-Vis absorption is accepted as a versatile and convenient method for the characterization of dissolved organic matter, which can provide information on the degree of humification and structural features of organic matter (Bai et al. 2008; Batista et al. 2016). To compare absorptivity among plant materials, specific absorbances of UV-Vis spectra were examined (Fig. 2). Spectra monotonously decrease as a function of increasing wavelength. Because the π-π^* electron transition occurs in the range of 254–280 nm, this wavelength range was selected to represent total aromaticity (Uyguner and Bekbolet 2005). In general, there were no obvious characterized peaks, but shoulder absorption peaks appeared. The two submerged plants, *Euryale ferox* L. and *Nelumbo nucifera* Gaertn.,

exhibited significant peaks, which indicated that the aromatic structure contents of the two plants were relatively high. The spectra of all of the emergent plants (*Alternanthera philoxeroides* (Mart.) Griseb., *Polygonum tortuosum* L., *Zizania latifolia* L., and *Phragmites australis* Trin.) and terrestrial plants (*Amaranthus tricolor* L., *Aeschynomene indica* L., and *Chenopodium glaucum* L.) contained shoulder peaks, which illustrated that these plants contained aromatic constituents.

The specific absorbances at 254 (SUVA$_{254}$) and 280 nm (SUVA$_{280}$) or the ratios of specific absorbances at various wavelengths, such as A$_{253/203}$, A$_{250/36}$, and A$_{465/665}$, have been related to the degree of humification (Chen et al. 2002; Rodríguez et al. 2016), aromaticity (Westerhoff et al. 1999), and molecular weight

Table 1 Percentage distribution of carbon in plant samples calculated by solid-state ^{13}C NMR spectroscopy

| Sample name	Type	NO	C chemical shift (ppm) (%)								Aliphatic C (%)	Aromatic C (%)
			0–45	45–65	65–90	90–110	110–145	145–160	160–190	190–220		
Alternanthera philoxeroides (Mart.) Griseb.	Emergent plants	1	13.19	13.49	40.85	12.07	9.26	3.29	7.63	0.25	79.60	12.55
Polygonum tortuosum L.		2	10.59	13.59	40.54	12.29	9.81	4.14	8.17	0.97	77.01	13.95
Zizania latifolia L.		3	12.07	16.43	45.85	12.06	5.74	1.79	5.96	0.06	86.41	7.53
Phragmites australis Trin.		4	13.56	15.03	41.22	11.84	8.96	2.59	6.88	0.11	81.64	11.56
Euryale ferox L.	Floating plants	5	19.97	14.85	30.18	8.83	11.26	2.80	12.23	0.13	73.82	14.06
Nelumbo nucifera Gaertn.		6	25.62	13.69	29.10	8.65	8.41	2.98	11.50	0.10	77.06	11.39
Hydrocharis dubia (Bl.) Backer.		7	17.37	13.74	40.62	10.52	7.01	1.21	9.62	0.06	82.24	8.22
Lemna minor L.		8	17.50	14.93	43.43	10.59	4.68	1.12	7.86	0.11	86.45	5.80
Nymphoides peltatum (Gmel.) O. Kuntze	Submerged plants	9	15.43	14.25	39.35	10.02	8.78	2.30	9.81	0.12	79.05	11.08
Trapa bispinosa Roxb.		10	13.75	13.02	39.99	11.24	10.03	2.26	9.91	0.03	78.01	12.29
Myriophyllum verticillatum L.		11	17.02	14.01	37.70	11.00	8.95	1.59	9.17	0.07	79.73	10.54
Potamogeton distinctus A. Benn.		12	15.75	13.93	41.52	10.82	7.79	1.69	8.34	0.03	82.02	9.48
Vallisneria natans (Lour.) Hara.		13	19.87	14.02	38.00	10.04	6.70	1.33	10.09	0.16	81.93	8.03
Hydrilla verticillata L.		14	19.16	14.22	38.28	10.74	6.69	1.38	9.67	0.11	82.40	8.07
Amaranthus tricolor L.	Terrestrial plants	15	17.71	14.66	39.89	10.33	4.88	1.66	11.13	0.05	82.59	6.53
Aeschynomene indica L.		16	12.60	14.80	44.52	12.45	6.51	2.45	6.65	0.07	84.38	8.96
Chenopodium glaucum L.		17	13.46	15.67	41.88	11.98	5.70	2.34	8.86	0.08	82.99	8.04

(Swietlik and Sikorska 2004). The UV-Vis absorbance parameters of different samples are shown in Table 2.

$SUVA_{254}$ and $SUVA_{280}$ are positively correlated with the humification degree of organic matter. Overall, the humification degrees of the four types of plants were in the sequence floating plants > terrestrial plants > submerged plants > emergent plants, and the degrees of humification in *Euryale ferox* L. and *Phragmites australis* Trin. were the greatest, while those of *Polygonum tortuosum* L. and *Potamogeton distinctus* A. Benn. were the least. Organic matter with greater degrees of humification can be transformed more efficiently into humic acid in water and sediment (Wang et al. 2009), which has a significant influence on the migration, toxicity, and storage of organic carbon. The $A_{253/203}$ ratio is indicative of the proportion of substituents on aromatic rings. $A_{253/203}$ ratios > 0.4 are indicative of aromatic rings that are mostly substituted by carbonyl, carboxyl, and hydroxyl groups, while ratios < 0.1 are indicative of aromatic rings that are unsubstituted (Korshin et al. 1997). All plant materials studied here exhibited high $A_{253/203}$ ratios, except *Amaranthus tricolor* L., *Polygonum tortuosum* L., and *Chenopodium glaucum* L. Other synthetic parameters that have been reported in the literature include the $A_{250/365}$ and $A_{465/665}$ ratios, both of which have been reported to be negatively correlated with molecular weight and aromaticity. Because high molecular weights undergo light absorption at longer wavelengths,

the value of $A_{250/365}$ is inversely proportional to molecular weight and aromaticity (Helms et al. 2008). *Phragmites australis* Trin exhibited a greater $A_{250/365}$ than other plants, which suggests less aromaticity and lower molecular weight, whereas an opposite trend was observed for *Nelumbo nucifera* Gaertn. The dissolved and degradation products of biomass with higher aromaticity contain more hydrophobic organic groups, which are easier to combine with hydrophobic organic compounds in water.

EEM spectral characteristics

The three-dimensional EEM fluorescence spectra of six representative plants provided spectral information about the chemical compositions of the plants (Fig. 3). The EEM peaks were divided into six regions (Table 3) (Fu et al. 2007; He et al. 2011; Mostofa et al. 2010): Fluorescence peaks in regions A (Ex/Em of 310–360/370–450 nm) and B (Ex/Em of 240–270/370–440 nm) have been attributed to fulvic acid-like materials. This fluorescence might be related to carbonyl and carboxyl groups. Region C (Ex/Em of 350–440/430–510 nm) and region D (Ex/Em of 280–288/420–455 nm) have been reported to represent humic acid-like materials and to be a function of the degree of humification. Region E (Ex/Em of 270–290/300–350 nm) and region F (Ex/Em of 270–290/300–320 nm) have been attributed to the presence of protein-like materials, in which fluorescence is due to tryptophan- and tyrosine-like substances, which is due to the
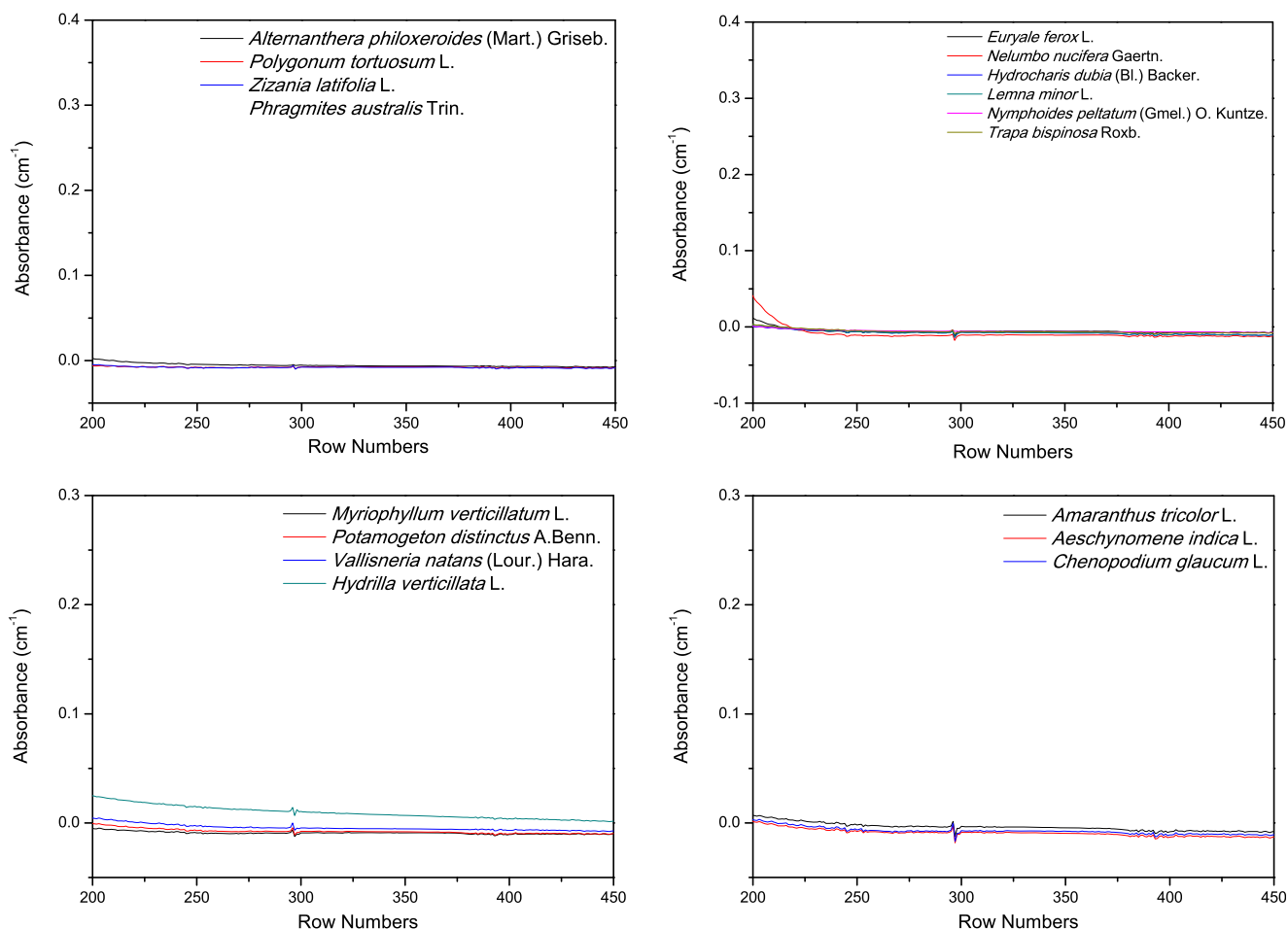
Fig. 2 UV-Vis spectra of plant materials from Tai Lake

| Table 2 UV-Vis absorbance of plant samples	Sample name	No	SUVA$_{254}$ (L/mg·m)	SUVA$_{280}$ (L/mg·m)	A$_{253}$/$_{203}$	A$_{250}$/$_{365}$	A$_{465}$/$_{665}$
	Alternanthera philoxeroides (Mart.) Griseb.	1	1.00	0.73	0.34	9.48	0.63
	Polygonum tortuosum L.	2	0.27	0.21	0.09	–	0.88
	Zizania latifolia L.	3	0.55	0.39	0.20	6.93	0.82
	Phragmites australis Trin.	4	0.51	0.37	0.19	47.89	0.85
	Euryale ferox L.	5	2.61	2.23	0.34	5.72	0.81
	Nelumbo nucifera Gaertn.	6	2.56	1.27	0.38	1.92	0.85
	Hydrocharis dubia (Bl.) Backer.	7	0.92	0.68	0.27	12.35	0.59
	Lemna minor L.	8	0.73	0.54	0.26	5.68	0.61
	Nymphoides peltatum (Gmel.) O. Kuntze	9	0.93	0.81	0.23	7.58	0.65
	Trapa bispinosa Roxb.	10	1.09	0.95	0.28	9.43	0.69
	Myriophyllum verticillatum L.	11	0.43	0.33	0.15	–	0.84
	Potamogeton distinctus A. Benn.	12	0.62	0.49	0.18	9.44	0.69
	Vallisneria natans (Lour.) Hara.	13	0.67	0.53	0.18	7.28	0.44
	Hydrilla verticillata L.	14	1.28	0.92	0.28	4.43	–
	Amaranthus tricolor L.	15	1.03	0.82	0.08	8.04	0.28
	Aeschynomene indica L.	16	0.88	0.70	0.18	8.80	0.55
	Chenopodium glaucum L.	17	0.85	0.61	0.09	9.70	0.57
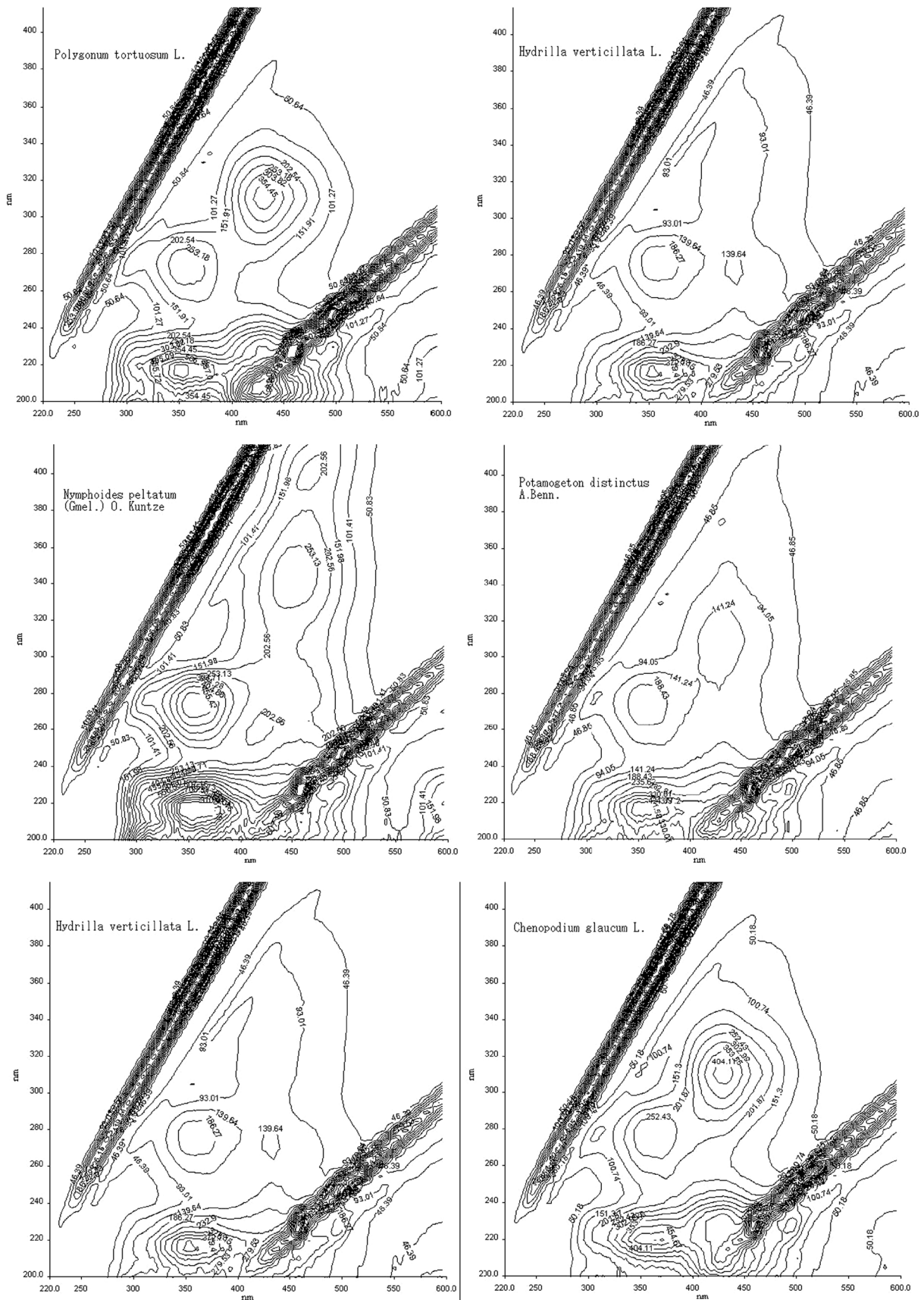
Fig. 3 EEM fluorescence spectra of some plant materials

structures of aromatic amino acids in plant materials (Song et al. 2017, 2018; Wang et al. 2009; Wu et al. 2003).

Fluorescence detected in EEM spectra can be applied in quantitative analyses, including the locations of peaks, intensity of fluorescence, and various ratios of intensities of peaks (Table 3). All plant materials studied exhibited peaks A and B, except *Nelumbo nucifera* Gaertn., *Vallisneria natans* (Lour.) Hara., and *Amaranthus tricolor* L., which exhibited peak B only. The existence of peaks A and B indicated that there were fulvic acid-like substances in the plant materials, and these peaks were related to carbonyl and carboxyl groups, consistent with the results of ^{13}C NMR. All plant materials studied exhibited peak E, and the materials of seven plants (*Polygonum tortuosum* L., *Zizania latifolia* L., *Hydrocharis dubia* (Bl.) Backer., *Phragmites australis* Trin., *Potamogeton distinctus* A. Benn., *Hydrilla verticillata* (Linn. f.) Royle, and *Chenopodium glaucum* L.) exhibited peak F. The presence of peaks E and F illustrates that there were protein-like substances in the plant materials. Peak C or D, or both, was also observed in *Hydrocharis dubia* (Bl.) Backer., *Nymphoides peltatum* (Gmel.) O. Kuntze., *Trapa bispinosa* Roxb., *Potamogeton distinctus* A. Benn., *Vallisneria natans* (Lour.) Hara., and *Chenopodium glaucum* L., and all six of these plants were submerged and floating plants, revealing that structural differences existed in different types of plants and submerged and terrestrial plants contained more humic acid-like materials than emergent and terrestrial plants. The locations of peaks varied slightly among the plant materials, which suggested that the chemical components of the plant materials were complex and varied among the plant materials. The intensities of the ratios of peaks A/E of *Polygonum tortuosum* L., *Phragmites australis* Trin., and *Chenopodium glaucum* L. were > 1.0, which indicated that there were more fulvic acid-like substances than tryptophan-like substances. The intensities of the ratios of peaks A/E of *Hydrocharis dubia* (Bl.) Backer, *Nymphoides peltatum* (Gmel.) O. Kuntze., *Trapa bispinosa* Roxb., and *Potamogeton distinctus* A. Benn. were also > 1.0, meaning that there were more fulvic acid-like substances than humic acid-like substances. According to the results of a previous study, variations in the intensity ratios of peaks in plant materials are due to differences among the chemical structures (Fu et al. 2010).

Discussion

Data for DSC and DTG peaks have been reported in previous literature (Guo et al. 2016b), and the DSC and DTG curves are presented in Fig. 4 (Guo et al. 2016b). DSC and DTG peaks were used to quantitatively explain the slow pyrolysis of plant biomass. The peak of heat absorbed by the plant samples (F1) was positively correlated ($r^2 = 0.507$; $p = 0.01$) with the peak of mass loss (G1) (Fig. 5a). The temperatures of F1 and G1

were 99–110 °C and 110–160 °C, respectively. It has been reported that below 110 °C, the physicochemical processes of soil and sediment organic matter are due to the glass transition and the rupture of bonds with water molecules (Schaumann and Bertmer 2008; Schaumann and Leboeuf 2005; Schaumann et al. 2005). Hence, it can be inferred that the corresponding thermal decomposition process was the melting process of small molecules or the glass transition process of high polymers and that a slight loss in mass was due to the removal of less thermally stable components.

The peak of heat release (Fx) was attained via a pyrolysis process that decomposed rapidly and released heat; this peak was well correlated with the value of $A_{253/203}$, and the correlation coefficient (r^2) was 0.388 ($p = 0.008$) (Fig. 5b). The temperature of Fx was 277–311 °C. As stated above, the $A_{253/203}$ ratio indicates the proportion of substituents on aromatic rings, $A_{253/203}$ ratios > 0.4 are indicative of aromatic rings that are mostly substituted by carbonyl, carboxyl, and hydroxyl groups (Korshin et al. 1997), and most plant materials exhibited higher $A_{253/203}$ ratios. This demonstrates that the release of heat increased as a function of substitution and that most condensation reactions were exothermic. It has been reported that there is an obvious exothermic curve of the polycondensation of furfuryl alcohol in acid media (Choura et al. 1997). Furthermore, in a study of the mechanism of polycondensation of dicyandiamide and formaldehyde, researchers also found an apparent heat-releasing phenomenon (Lin 2004). We concluded that this pyrolysis process was mainly based on the condensation reactions between molecules, forming heavy components and solid products and releasing heat.

For a better understanding of changes in the structures of plant materials during pyrolysis, loss of mass (DTG) combined with three-dimensional fluorescence analysis was used for quantitative analysis. The correlation coefficient (r^2) was 0.236 ($p = 0.048$) between peak A and the peak of mass loss (G3) (Fig. 5c). The temperature of G3 was 230–340 °C. Peak A has been reported to represent fulvic acid-like materials and might be related to carbonyl and carboxyl groups. Additionally, most plants exhibited fulvic acid-like material fluorescence peaks. Similar peaks were found in coal pyrolysis at approximately this temperature range (Bhagavatula et al. 2016; Goergens et al. 2013). This pyrolysis process mainly involves the splitting of aromatic structural unit bonds, aliphatic hydrocarbon side chains, and oxygen-containing functional groups. In addition, the unstable branch carbon functional groups had been broken down in the previous process, and the peak temperature range was 210–260 °C. ^{13}C NMR spectral analysis also confirmed that all plant samples contained more and fewer hydroxyl carbons and carboxyl carbons, respectively. Therefore, we deduced that the pyrolysis process of G3 primarily represents aromatic carbonyl removal and splitting of ether bonds, carbonyl groups, and oxygen heterocycles, mainly by means of decomposition, depolymerization, and polycondensation.

Table 3 EEM fluorescence spectral parameters of plant samples (blank means no peak was observed)

| Sample name	No	Peak A Ex/Em	Int	Peak B Ex/Em	Int	Peak C Ex/Em	Int	Peak D Ex/Em	Int	Peak E Ex/Em	Int	Peak F Ex/Em	Int	Peak intensity ratio A/B	A/C	A/D	A/E	A/F	E/F
Alternanthera philoxeroides (Mart.) Griseb.	1	310/431	139.2	215/364.5	828.7					275/356	353.3			0.17			0.39		
Polygonum tortuosum L.	2	310/430.5	386.3	215/353.5	649.9					275/350.5	286.6	280/310	197.6	0.59			1.35	1.95	1.45
Zizania latifolia L.	3	310/432	271.9	215/351.5	778.8					270/351.5	343.8	280/311	213.7	0.35			0.79	1.27	1.61
Phragmites australis Trin.	4	310/432	633.6	215/353	1000.6					275/350	542.9			0.63			1.17		
Euryale ferox L.	5	320/430.5	201.9	215/351.5	538.8					270/354	382.3			0.37			0.53		
Nelumbo nucifera Gaertn.	6			225/361.5	1001.9					270/382.5	1001.6								
Hydrocharis dubia (Bl.) Backer.	7	315/432.5	150.3	215/352.5	436.1	350/398	108.8	280/428	143.2	275/358	207.1	280/311	151.7	0.34	1.38	1.05	0.73	0.99	1.37
Lemna minor L.	8	335/419	136.8	215/350	454.1					275/352.5	195.8	280/310	163.8	0.30			0.70	0.84	1.20
Nymphoides peltatum (Gmel.) O. Kuntze	9	345/452.5	286.6	220/346.5	1000.5	405/470	220.8	280/449	241.5	275/353	496.7			0.29	1.30	1.19	0.58		
Trapa bispinosa Roxb.	10	310/435.5	115.9	215/356.5	581.8	360/471	99.3			270/352.5	269.2			0.20	1.17		0.43		
Myriophyllum verticillatum L.	11	310/432.5	217.9	215/351	991.3					275/356	381.3			0.22			0.57		
Potamogeton distinctus A. Benn.	12	310/430.5	180.0	215/354.5	509.0	375/431	97.0			275/350	218.6	280/311	150.1	0.35	1.86		0.82	1.20	1.46
Vallisneria natans (Lour.) Hara.	13			220/347.5	575.7	375/431	107.2	270/433.5	141.3	275/352.5	237.4								
Hydrilla verticillata L.	14	330/432	124.1	215/356	483.1			275/431	146.2	275/353	210.3	280/311	130.2	0.26		0.85	0.59	0.95	1.62
Amaranthus tricolor L.	15			220/367.5	853.3					275/360.5	576.5								
Aeschynomene indica L.	16	310/430.5	434.3	220/346.5	1001.3					275/356.5	482.2			0.43			0.90		
Chenopodium glaucum L.	17	310/429	432.6	220/370.5	514.6					280/366.5	292.3	280/310	163.3	0.84			1.48	2.65	1.79
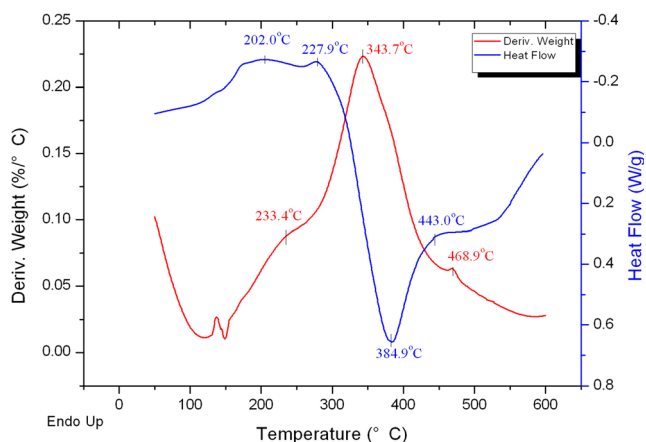
Fig. 4 DSC and DTG overlay analyses of lignin (DSC, differential scanning calorimetry; DTG derivative thermogravimetric analysis) (Guo et al. 2016b)

Conclusions

Based on the results of this study, the following conclusions can be drawn:

1. ^{13}C NMR measurements showed that the proportions of aliphatic carbons (ranging from 73.82 to 86.45%) were substantially greater than those of aromatic carbons (ranging from 5.80 to 14.06%) in plant samples. The plant types with the highest mean contents of aliphatic carbon and aromatic carbon were terrestrial plants and emergent plants, with values of 83.32 and 11.40%, respectively.

2. The results of UV-Vis spectroscopy showed the order of humification degree in the four types of plants was floating plants > terrestrial plants > submerged plants > emergent plants. The parameter with the best correlation with the release of heat stage (277–311 °C) was the $A_{253/203}$ ratio, and the exothermic process was mainly due to polycondensation between molecules.
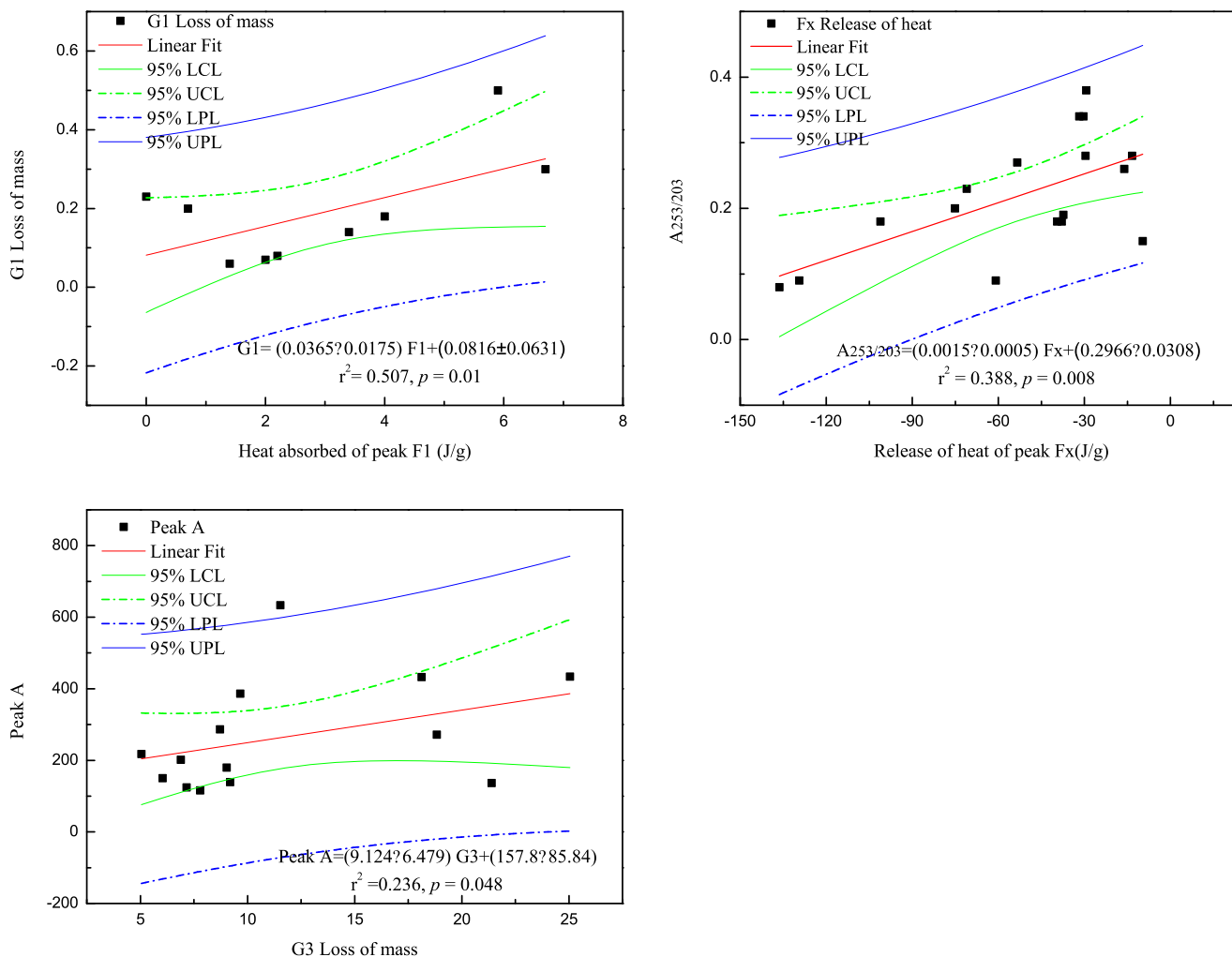
Fig. 5 Scatter plots, general linear models, and coefficients of determination (r^2): peak F1 as a function of peak G1 (**a**); peak Fx as a function of $A_{253/203}$ (**b**); peak G3 as a function of peak A (**c**)

3. Most plant materials exhibited fulvic acid-like substance and protein-like substance fluorescence peaks according to the EEM analysis. The fulvic acid-like fluorescence peak and loss of mass stage (230–340 °C) showed good correlation; this stage was mainly due to the loss of aromatic carbonyls and oxygen heterocycles as well as splitting of ether bonds.

4. There was a significant linear correlation between the absorption of heat stage (99–110 °C) and the loss of mass stage (110–160 °C); this stage was a melting process of small molecules or a glass transition process of high polymers.

5. The use of thermal and spectroscopic analyses to characterize NOM proved to be an effective technique. The results will be conducive to understanding every stage of slow pyrolysis and interpreting thermograms of NOM. Furthermore, this method will be valuable to reveal the intrinsic structure and mechanism of the influence of NOM on environmental behavior.

References

Aiken GR, Hsu H (2011) Influence of dissolved organic matter on the environmental fate of metals, nanoparticles, and colloids. Environ Sci Technol 45:3196–3201

Alexis MA, Rumpel C, Knicker H, Leifeld J, Rasse D, Péchot N, Bardoux G, Mariotti A (2010) Thermal alteration of organic matter during a shrubland fire: a field study. Org Geochem 41:690–697

Ali M, Bhatia A, Kazmi AA, Ahmed N (2012) Characterization of high rate composting of vegetable market waste using Fourier transform-infrared (FT-IR) and thermal studies in three different seasons. Biodegradation 23:231–242

And JFH, Ohno T (2007) Characterization of fresh and decomposed dissolved organic matter using excitation−emission matrix fluorescence spectroscopy and multiway analysis. J Agric Food Chem 55: 2121–2128

And SK, Xing B (2008) Humic acid fractionation upon sequential adsorption onto goethite. Langmuir Acs J Surf Colloids 24:2525–2531

Antisari LV, Dell'Abate MT, Buscaroli A, Gherardi M, Nisini L, Vianello G (2010) Role of soil organic matter characteristics in a pedological survey: "Bosco Frattona" natural reserve (Site of Community Importance, Italy) case study. Geoderma 156:302–315

Bai YC, Wu FC, Liu CQ, Li W, Guo JY, Fu PQ, Xing BS, Zheng J (2008) Ultraviolet absorbance titration for determining stability constants of humic substances with Cu(II) and Hg(II). Anal Chim Acta 616:115–121

Batista AP, Teixeira AC, Cooper WJ, Cottrell BA (2016) Correlating the chemical and spectroscopic characteristics of natural organic matter with the photodegradation of sulfamerazine. Water Res 93:20–29

Bhagavatula A, Shah N, Honaker R (2016) Estimating the pyrolysis kinetic parameters of coal, biomass, and their blends: a comparative study. Energ Fuel 30:10045–10054

Birdwell JE, Engel AS (2010) Characterization of dissolved organic matter in cave and spring waters using UV-Vis absorbance and fluorescence spectroscopy. Org Geochem 41:270–280

Chen J, Gu B, Leboeuf EJ, Pan H, Dai S (2002) Spectroscopic characterization of the structural and functional properties of natural organic matter fractions. Chemosphere 48:59–68

Choura M, Belgacem NM, Gandini A (1997) The acid-catalyzed polycondensation of furfuryl alcohol: old puzzles unravelled. Macromol Symp 122:263–268

Dell'Abate MT, Benedetti A, Brookes PC (2015) Hyphenated techniques of thermal analysis for characterisation of soil humic substances. J Sep Sci 26:433–440

Fu P, Wu F, Liu C, Wang F, Li W, Yue L, Guo Q (2007) Fluorescence characterization of dissolved organic matter in an urban river and its complexation with Hg(II). Appl Geochem 22:1668–1679

Fu PQ, Mostofa KMG, Wu FC, Liu CQ, Wen L, Liao HQ, Wang LY, Jing W, Yi M (2010) Excitation-emission matrix characterization of dissolved organic matter sources in two eutrophic lakes (Southwestern China Plateau). Geochem J 44:99–112

Goergens M, Knoetze JH, Aboyade AO (2013) Thermogravimetric study of the pyrolysis characteristics and kinetics of coal blends with corn and sugarcane residues. Fuel Process Technol 106:310–320

Guo F, Mu Y, Chen C, Liao H, Bai Y (2016a) Thermal and spectral characterization of anaerobic thermal behavior patterns in a lacustrine sediment core. Environ Sci Pollut Res Int 23:19949–19957

Guo F, Wu F, Mu Y, Hu Y, Zhao X, Meng W, Giesy JP, Lin Y (2016b) Characterization of organic matter of plants from lakes by thermal analysis in a N2 atmosphere. Sci Rep 6:22877

He XS, Xi BD, Wei ZM, Jiang YH, Yang Y, An D, Cao JL, Liu HL (2011) Fluorescence excitation–emission matrix spectroscopy with regional integration analysis for characterizing composition and transformation of dissolved organic matter in landfill leachates. J Hazard Mater 190:293–299

Helms JR, Stubbins A, Ritchie JD, Minor EC, Kieber DJ, Mopper K (2008) Absorption spectral slopes and slope ratios as indicators of molecular weight, source, and photobleaching of chromophoric dissolved organic matter. Limnol Oceanogr 53:955–969

Jansson M (1998) Nutrient limitation and bacteria — phytoplankton interactions in humic lakes. Springer, Berlin Heidelberg, pp 177–195

Korshin GV, Benjamin MM, Sletten RS (1997) Adsorption of natural organic matter (NOM) on iron oxide: effects on NOM composition and formation of organo-halide compounds during chlorination. Water Res 31:1643–1650

Lin F (2004) Development and prospects of the flocculant of dicyandiamine-formaldehyde condensation product type. Industrial Water Treatment 77:459–463

Lin Y, Wu F, Bai Y, Xie F, CAO Z, Su H (2011) Isolation and characterization of standard fulvic acids from soil and sediments in China. Res Environ Sci 24:1142–1148

Lopez-Capel E, Abbott GD, Thomas KM, Manning DAC (2006) Coupling of thermal analysis with quadrupole mass spectrometry and isotope ratio mass spectrometry for simultaneous determination of evolved gases and their carbon isotopic composition. J Anal Appl Pyrolysis 75:82–89

Mostofa KMG, Wu F, Liu CQ, Fang WL, Yuan J, Ying WL, Wen L, Yi M (2010) Characterization of Nanming River (southwestern China) sewerage-impacted pollution using an excitation-emission matrix and PARAFAC. Limnology 11:217–231

Prado AGS, Pertusatti J, Nunes AR (2011) Aspects of protonation and deprotonation of humic scid durface on molecular conformation. J Braz Chem Soc 22:1478–1483

Ravindran B, Sravani R, Mandal AB, Contreras-Ramos SM, Sekaran G (2013) Instrumental evidence for biodegradation of tannery waste during vermicomposting process using Eudrilus eugeniae. J Therm Anal Calorim 111:1675–1684

Rodríguez FJ, Schlenger P, García-Valverde M (2016) Monitoring changes in the structure and properties of humic substances following ozonation using UV–Vis, FTIR and 1 H NMR techniques. Sci Total Environ 541:623–637

Schaumann GE, Bertmer M (2008) Do water molecules bridge soil organic matter molecule segments. Eur J Soil Sci 59:423–429

Schaumann GE, Leboeuf EJ (2005) Glass transitions in peat: their relevance and the impact of water. Environ Sci Technol 39:800–806

Schaumann GE, Leboeuf EJ, Delapp R, Hurraß J (2005) Thermomechanical analysis of air-dried whole soil samples. Thermochim Acta 436:83–89

Sheng GP, Yu HQ (2006) Characterization of extracellular polymeric substances of aerobic and anaerobic sludge using three-dimensional excitation and emission matrix fluorescence spectroscopy. Water Res 40:1233–1239

Song F, Wu F, Guo F, Wang H, Feng W, Zhou M, Deng Y, Bai Y, Xing B, Giesy JP (2017) Interactions between stepwise-eluted sub-fractions of fulvic acids and protons revealed by fluorescence titration combined with EEM-PARAFAC. Sci Total Environ 605–606:58–65

Song F, Wu F, Xing B, Li T, Feng W, Giesy JP, Guo W, Wang H, Liu S, Bai Y (2018) Protonation-dependent heterogeneity in fluorescent binding sites in sub-fractions of fulvic acid using principle component analysis and two-dimensional correlation spectroscopy. Sci Total Environ 616–617:1279–1287

Swietlik J, Sikorska E (2004) Application of fluorescence spectroscopy in the studies of natural organic matter fractions reactivity with chlorine dioxide and ozone. Water Res 38:3791–3799

Uyguner CS, Bekbolet M (2005) Implementation of spectroscopic parameters for practical monitoring of natural organic matter. Desalination 176:47–55

Wang L, Wu F, Zhang R, Li W, Liao H (2009) Characterization of dissolved organic matter fractions from Lake Hongfeng, Southwestern China Plateau. J Environ Sci 21:581–588

Westerhoff P, Aiken G, Amy G, Debroux J (1999) Relationships between the structure of natural organic matter and its reactivity towards molecular ozone and hydroxyl radicals. Water Res 33:2265–2276

Wilson MA, Barron PF, Gillam AH (1981) The structure of freshwater humic substances as revealed by 13C-NMR spectroscopy. Geochim Cosmochim Acta 45:1743–1750

Wu FC, Evans RD, Dillon PJ (2003) Separation and characterization of NOM by high-performance liquid chromatography and on-line three-dimensional excitation emission matrix fluorescence detection. Environ Sci Technol 37:3687–3693